

# Simple magnetic reconnection example

Allen H Boozer and Todd Elder  
*Columbia University, New York, NY 10027*  
*ahb17@columbia.edu*  
(Dated: June 12, 2022)

In laboratory and natural plasmas of practical interest, the smallest spatial scale  $\Delta_d$  over which magnetic field lines are distinguishable on the time scale set by an ideal evolution differs enormously from the scale  $a$  of magnetic reconnection across the field lines. In the solar corona, plasma resistivity gives  $a/\Delta_d \sim 10^{12}$ , which is the magnetic Reynold number  $R_m$ . The standard resolution of the paradox of disparate time scales is for the current density  $j$  associated with the reconnecting field  $B_{rec}$  to be concentrated by the ideal evolution, so  $j \sim B_{rec}/\mu_0\Delta_d$ , an amplification by a factor  $R_m$ . A second resolution is for the ideal evolution to increase the ratio of the maximum to minimum separation between two arbitrarily chosen magnetic field lines,  $\Delta_{max}/\Delta_{min}$ , when calculated at various points in time. Reconnection becomes inevitable when  $\Delta_{max}/\Delta_{min} \sim R_m$ . As demonstrated using a simple model of the solar corona, the natural rate of increase in time is linear for the current density but exponential for  $\Delta_{max}/\Delta_{min}$ . Reconnection occurs on a time scale and with a current density enhanced by only  $\ln((a/\Delta_d))$  from the ideal evolution time and from the current density  $B_{rec}/\mu_0a$ . In both resolutions of the paradox of disparate time scales, once a sufficient region has undergone reconnection, the magnetic field loses force balance and evolves ideally on an Alfvén transit time. This ideal evolution generally expands the region in which  $\Delta_{max}/\Delta_{min}$  is large.

## I. INTRODUCTION

The evolution of a magnetic field embedded in a hot plasma would be expected to be accurately ap-

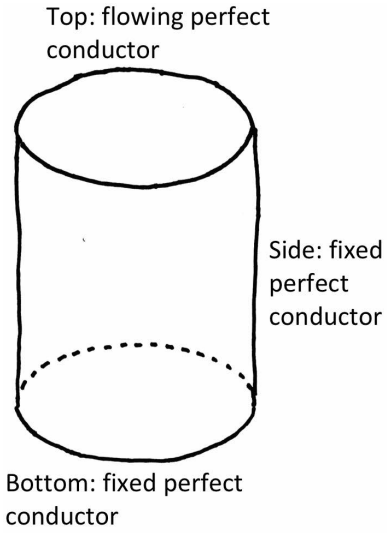


FIG. 1: A perfectly conducting cylinder of height  $L$  and radius  $a$  encloses an ideal pressureless plasma. All the sides of the cylinder are fixed except the top, which flows with a specified velocity  $\vec{v}_t$ . Initially,  $\vec{B} = B_0\hat{z}$ . The magnetic evolution is assumed to be ideal, Equation (1). Each point  $x_0 = r_0 \cos \theta_0$ ,  $y_0 = r_0 \sin \theta_0$  on the bottom of the cylinder defines a line of  $\vec{B}$  that intercepts a specific point in the top  $\vec{x}_t(x_0, y_0, t)$  with  $\partial \vec{x}_t / \partial t = \vec{v}_t$ .

proximated by the ideal-evolution equation

$$\frac{\partial \vec{B}}{\partial t} = \vec{\nabla} \times (\vec{u}_\perp \times \vec{B}). \quad (1)$$

Newcomb [1] showed in 1958 that in an ideal evolution the magnetic field lines move with a velocity  $\vec{u}_\perp$  and cannot break. The importance of departures from this equation due to resistivity  $\eta$  scale as  $1/R_m$ , where the magnetic Reynolds number is

$$R_m \equiv \left( \frac{a^2}{\eta/\mu_0} \right) \left( \frac{u_\perp}{a} \right) = \frac{\mu_0 u_\perp}{\eta} a, \quad (2)$$

the ratio of the resistive to the evolution time scale. In the solar corona,  $R_m \sim 10^{12}$ . Nevertheless, magnetic field lines are observed to undergo remarkably rapid “*severing and reconnection*,” which was the 1956 definition of magnetic reconnection by Parker and Krook [2].

The speed and prevalence of magnetic reconnection are of great practical importance in laboratory and naturally occurring plasmas. Both the speed and the prevalence are so great that they must derive from the properties of Equation (1) for the ideal evolution of a magnetic field.

In 1988, Schindler, Hesse, and Birn described the problem of reconnection in their well-known paper [3]. “*If the nonideality is spatially extended (diffusion),  $R_m$  has to be of the order of 1 for the breakdown of magnetic connection to have a significant effect on the plasma dynamics. In contrast to diffusion, GMR (General Magnetic Reconnection) determines the plasma dynamics in situations where  $R_m \gg 1$ . This becomes possible as a consequence of the localization of the nonideality. In fact, if*

one computes a local Reynolds number using the dimension of the diffusion region instead of the overall length  $L$  ( $L = a$  in our notation), one finds a value of the order of 1.”

The statement by Schindler et al is correct, but they only considered one of two options for resolving a paradox. In their resolution, the ideal evolution concentrates the current density  $j$  into a narrow region  $\Delta_d \sim a/R_m$ , which amplifies the current density by a factor of  $R_m$  from its natural magnitude  $j \sim B_{rec}/\mu_0 a$ . The spatial scale across the magnetic field lines in which the field  $B_{rec}$  reconnects is  $a$ . To reconnect a large volume of magnetic field lines, the ideal evolution must not only create but also maintain the  $R_m$  amplification. This option has been the paradigm of reconnection theory since its inception.

The other option for resolving the paradox considers the ratio of separations of two arbitrarily chosen magnetic field lines. At any particular time, these two lines have a maximum and a minimum separation as they traverse the system. An ideal evolution changes the ratio  $\Delta_{max}/\Delta_{min}$  as time advances. As will be shown using a simple model of magnetic evolution in the solar corona, Figure 1, essentially any credible ideal evolution causes  $\Delta_{max}/\Delta_{min}$  to increase exponentially on the time scale of the ideal evolution. On the other hand, the current-density increase, which was emphasized by Schindler et al, increases only linearly in time, far too slowly to have a significant effect on the local magnetic Reynolds number. Once  $\Delta_{max}/\Delta_{min} \sim R_m$  reconnection becomes inevitable. After reconnection starts, the magnetic field can lose force balance, which gives an ideal evolution on an Alfvénic time scale,  $L/V_A$ , where  $L$  the distance required for a magnetic field line to traverse the system. This ideal evolution causes an additional increase in  $\Delta_{max}/\Delta_{min}$ .

Loops of magnetic field lines in the solar corona provide an especially simple example of how an ideal evolution can rapidly create conditions that make reconnection inevitable. The two ends of the loops are forced to move with a velocity determined photospheric motions. The fundamental simplicity makes coronal reconnection archetypal for magnetic reconnection in general.

A model of the ideal evolution of the coronal magnetic field is illustrated in Figure 1. The plasma is confined by a perfectly conducting cylinder of radius  $a$  and height  $L$ , which gives well-posed boundary conditions. The conducting surfaces are rigid except for a flowing top-surface. That flow must have the form

$$\vec{v}_t = \hat{z} \times \vec{\nabla} h_t(r, \theta, t). \quad (3)$$

in order not to compress the initial field  $\vec{B}_0 = B_0 \hat{z}$  with  $B_0$  a constant. The stream function  $h_t$  is spec-

ified, and represents the photospheric motion at one interception of the loop. For simplicity, the flow at the other photospheric interception is taken to be zero. The effect of the flow is to produce a magnetic field orthogonal to  $\vec{B}_0$ .

The model illustrated in Figure 1 is closely related to the well-known Parker Problem [4], which was recently reviewed by Pontin and Hornig [5]. It is also a simplified version of reconnection models of the corona published by Boozer [6] and independently by Reid et al [7] in 2018. Although these two models are similar, the mathematical cause for reconnection emphasized in these papers is different. Reid et al [7] used an anomalous resistivity to ensure “*that resistivity, as opposed to a numerical diffusion, is responsible for any magnetic reconnection.*” Boozer’s paper and his more recent work [8–11] emphasized that an imposed chaotic flow  $\vec{v}_t$  would make magnetic reconnection exponentially sensitive to any departures from an ideal evolution.

The flow  $\vec{v}_t$  is deterministic but, using standard terminology, is chaotic when neighboring streamlines have a separation that increases exponentially with time. Articles on the mathematics of deterministic chaos and topological mixing can easily be found on the web, but their importance to this paper is only that such effects are common. The argument that energy prevents a chaotic ideal flow of the magnetic field lines applies to two- but not to three-dimensional systems [11].

Essentially any stream function  $h_t(x, y, t)$  with non-trivial dependencies on all three variables gives chaos. Section II gives examples that are non-zero only for  $r < a$ . In effect,  $a$  represents the maximum coherence scale of the photospheric flow across the magnetic field lines that is being modeled. The spatial scale  $b$  of the variation in  $h_t(x, y, t)$  could be much shorter than  $a$ . When  $b \ll a$ , the reconnection proceeds on a time scale comparable to the evolution time  $b/v_t$  only over the scale  $b$ . On larger spatial scales, reconnection proceeds at a much slower quasi-diffusive rate. Flows with  $b \ll a$ , such as turbulent flows, have much slower reconnection for a given flow speed than those with  $b \sim a$ , [11]. The flows we explicitly integrate have  $b \sim a$ , which not only makes the reconnection fast over a scale comparable to  $a$  but are also much easier to integrate.

Figure 2a illustrates the effect of a simple  $\vec{v}_t$  that is chaotic. Almost all choices of  $h_t$  that have non-trivial  $x$ ,  $y$ , and  $t$  dependencies are chaotic. One hundred streamlines are started on the perimeter of the small black circle, but as the red dots illustrate, these hundred streamlines spread over most of the region  $r < a$  after only five periods of the flow. The perimeter of the small circle defines a tube in time with fixed area. The cross section of this tube be-

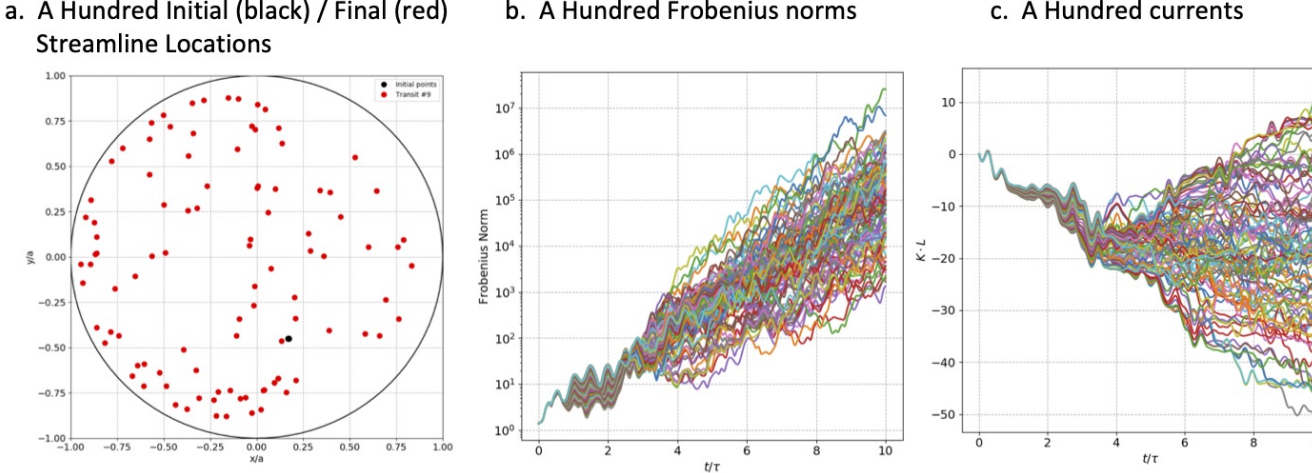


FIG. 2: Streamline properties are illustrated for the stream function of Equation (10) with  $c_0 = 0$ ,  $c_1 = c_2 = c_3 = 1/4$ ,  $\omega_1 = 6\pi$ ,  $\omega_2 = 4\pi$ ,  $\omega_3 = 0$ , and  $\lambda^2 = 0$ . Figure 2a is plot of a hundred streamlines started on the perimeter of the small black circle, which has a radius of  $a/1000$  and is centered at an arbitrary point,  $x/a = 0.17$  and  $y/s = -0.45$ . The red dots are the locations of the hundred streamlines after nine transits. The locations are widely scattered within the region  $r < a$  in which the derivatives of the stream function are non-zero. Figure 2b shows the evolution of the Frobenius norm, Equation (8) for these hundred streamlines. The Frobenius norm is a precise measure of the separation of neighboring trajectories. As expected in a chaotic flow, the Frobenius norm tends to increase exponentially with time. Figure 2c shows the evolution of the force-free current  $K \equiv \mu_0 j_{||}/B$  times the length of the cylinder  $L$  given by Equation (33) for each of the hundred field lines that initially intercepted the top surface on the perimeter of the black circle.

comes convoluted in the extreme; all the red dots must lie on the perimeter of the tube.

The precise mathematical measure of the separation of streamlines in the neighborhood of any given line is the Frobenius norm of a Jacobian matrix, which is explained in Section II. Despite the closeness of their starting points the hundred trajectories have a wide range of Frobenius norms, which all have an exponential increase with time, Figure 2b.

Two physical effects make two field lines that pass closer than a distance  $\Delta_d$  of each other indistinguishable in an evolution. (1) Electron inertia makes evolving field lines indistinguishable when  $\Delta_d \lesssim c/\omega_{pe}$  as shown in Appendix C of [10]. This produces reconnection in the same way that a finite numerical grid produces reconnection. 2. Resistivity produces field-line diffusion with a coefficient  $\eta/\mu_0$ , which is physically analogous to the numerical diffusion mentioned by Reid et al [7]. When two field lines are separated by a distance  $\Delta_d$  with  $(\mu_0/\eta)\Delta_d^2 < \Delta_d/|\vec{u}_\perp|$ , resistivity makes the two lines indistinguishable. This is equivalent to the local magnetic Reynolds number being less than unity. Magnetic reconnection occurs over the scale  $a$  when two magnetic field lines that have a closest approach  $\Delta_d$  separate to a distance comparable to  $a$  as they traverse the cylinder from the bottom to the top. The similarity of numerical to non-ideal effects was

invoked in 2009 by Pariat, Antiochos, and DeVore [12] to support their reconnection simulations based on ideal evolution equations.

For magnetic reconnection, the principle issue is the ratio of the maximum distance to the minimum distance between two magnetic field lines. This ratio is at least as large as the ratio of the separations at their top and bottom intercepts with the conducting cylinder. The top-bottom ratio is easy to calculate and can be used to demonstrate the inevitability of reconnection. Reid et al in their 2020 paper [13] drove their system with an integrable flow at one end, but the magnetic field lines became chaotic anyway after ideal kink instabilities occurred.

As anyone who has attended a recent meeting on reconnection knows, the relevance of exponentiation to the prevalence and speed of reconnection has not yet become a part of the paradigm of the field. Nonetheless, once streamlines exponentiate apart, magnetic reconnection is inevitable over the separation that streamlines that are initially close can reach. Figure 2a illustrates that initially close streamlines can reach a large fraction of the points  $r < a$  in a simple chaotic flow. The time scale for reconnection depends only logarithmically on the smallness of non-ideal effects multiplied by the time scale of the ideal evolution.

An ideal evolution that is leading inevitably to

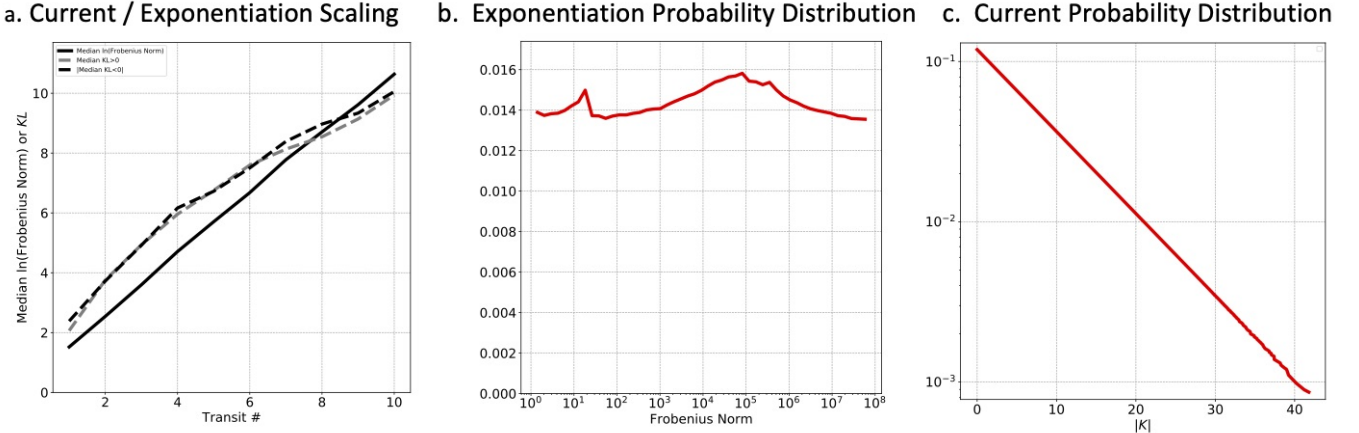


FIG. 3: Data was gathered from a thousand starting points that were uniformly spread over  $r < a$  to determine characteristic properties of the Frobenius norm, which measures the exponentiation of streamline separation, and the current density  $K$  times the length of the cylinder  $L$ . Figure 3a shows the evolution of the median of the natural logarithm of the Frobenius norm in solid black, the median value of  $|KL|$  in a dashed gray (positive), and dashed black (negative) line. All three increase approximately linearly in time. The probability distribution of the Frobenius norm is shown in Figure 3b and of the current density distribution in Figure 3c. All of the calculations used data after ten transits.

a reconnection has remarkable features. During periods when the evolution is slow compared to the Alfvén transit time,  $L/V_A$ , integrations of the streamlines in the top of the cylinder will be found to give essentially all of the information about the plasma until it reaches the reconnecting state:

1. The exponentiation in magnetic-field-line separation directly produced by the flow.

The separation of neighboring field lines is measured by the Frobenius norm. The median Frobenius norm increases exponentially with time, Figure 3a.

2. The detailed force-free current profile,  $K \equiv \mu_0 j_{||}/B$ , throughout the plasma, Equation (33).

The current-density in the plasma lies in ribbon-like sheets along the magnetic field, which tend become thinner and broader, Figure 4, as time advances. The median magnitude of the current density increases only linearly in time, Figure 3a. The maximum current density also increases only linearly.

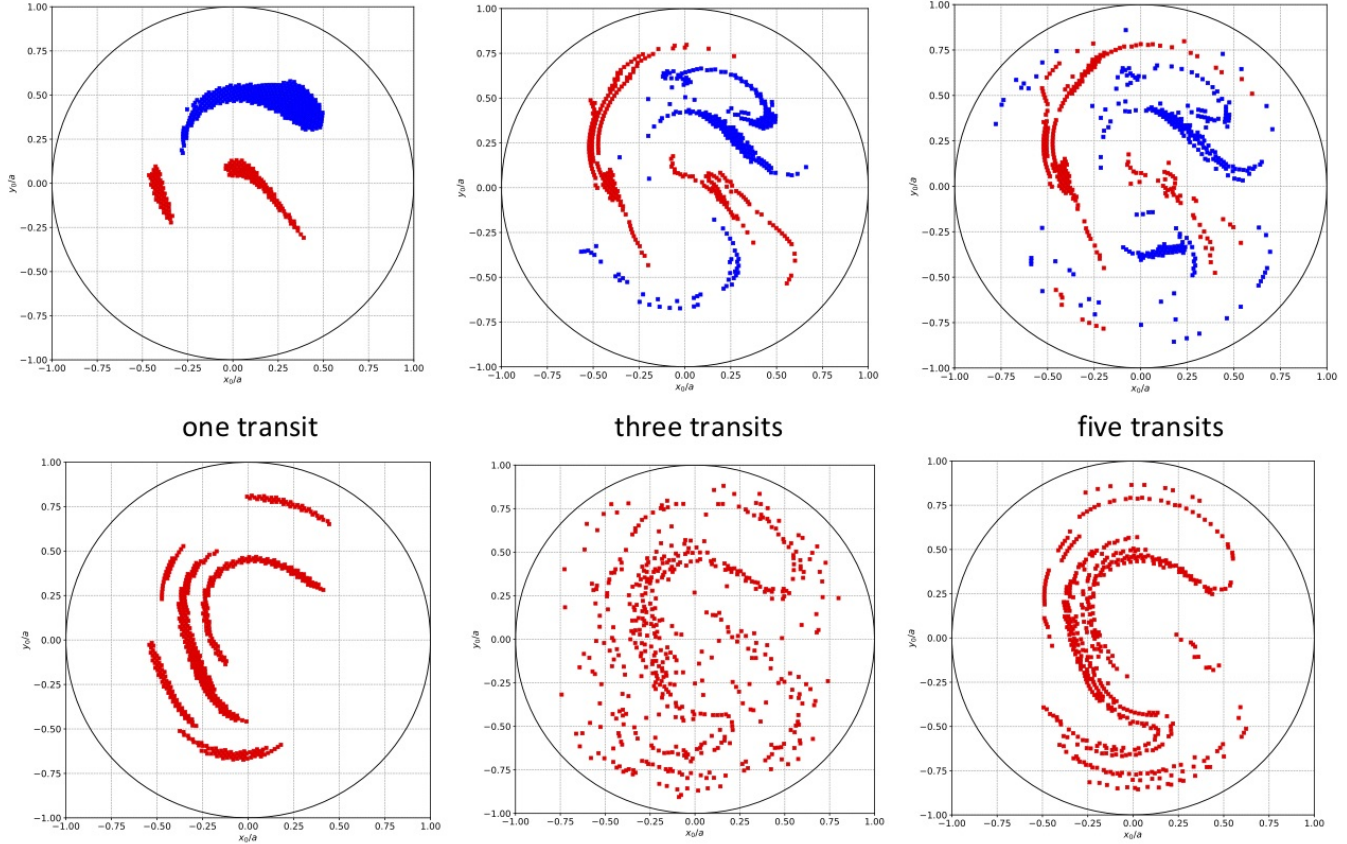
3. The power required to drive the flow, Equation (59).
4. The ratio of the resistive destruction of the magnetic flux relative to its creation, Equation (42). Resistive diffusion is found to be negligible when  $R_m \gg 1$ .

5. The magnetic helicity enclosed by the perfectly conducting cylinder, which can predict when the eruption of flux tubes must take place, Section VI.

Parker and Krook's definition of reconnection is fundamentally different in chaotic magnetic fields than the definition used by Reid et al [13] in their 2020 paper. Reid et al used the rate at which magnetic flux is directly reconnected by resistivity, “*the integral along a field line of the component of the electric field parallel to the magnetic field*,”  $\int E_{||} d\ell$ . This was based on the assertion that this is “*the necessary and sufficient condition for reconnection*,” which is a standard assumption in reconnection theory. The most compelling argument for this assertion was the 1988 paper by Schindler et al [3]. Their resolution of the reconnection paradox is equivalent to assuming reconnection rate is the resistive part of the integral  $\int E_{||} d\ell$ .

Reid et al [13] found that the resistive part of the integral  $\int E_{||} d\ell$  has a weak correlation with the quasi-squashing factor, “*the degree with which initially neighboring magnetic field lines diverge as they transverse a system*” [14, 15]. The quasi-squashing factor measures the deformation of a field line mapping between two surfaces, such as the top and bottom of the cylinder in Figure 1, which in the model of Figure 1 is given by the chaos in  $\vec{v}_t$ . The general definition of chaotic magnetic field lines is an exponentially large Singular Value of the  $3 \times 3$  Jacobian matrix  $\partial \vec{x}/\partial \vec{x}_0$ , where  $\partial \vec{x}/\partial \vec{x}_0, \ell)/\partial \ell = \hat{b}(\vec{x})$ ,

### Locations of large currents densities



### Locations of rapid streamline separations

FIG. 4: Ten thousand starting points were uniformly spread over  $r < a$ . The top row is the locations of the five hundred points that had the largest current density  $|K|$  after one, three, and five transits. Red implies  $K$  is negative and blue positive. The bottom row is the locations of the five hundred points that had the largest Frobenius norm, which measures the rapidity of streamline separation. The correlation between a large  $K$  and a large Frobenius norm is weak. The regions with a high current density  $K$  tend to become long and thin, but small regions that have a correlated current density do not entirely disappear. Figure 2c also illustrates this.

$\vec{x}_0 \equiv \vec{x}(\vec{x}_0, \ell = 0)$ , and  $\hat{b} = \vec{B}/B$ . Chaos in the magnetic field lines determines the exponential enhancement of reconnection and can be larger than the chaos in footpoint flows. The correlation between large values of the current density  $|K|$  and large values of the Frobenius norm is weak in an ideal evolution, Figure 4, in agreement with the result of Reid et al.

The Parker Problem, which was originally stated [4] by Eugene Parker in 1978 and recently reviewed by Pontin and Hornig [5], is similar to that defined by Figure 1. The focus of studies on the Parker Problem has been on the formation of tangential discontinuities, which are places where  $|\vec{j}| \rightarrow \infty$ . But, it is much easier for an ideal magnetic evolu-

tion to develop a  $\Delta_{max}/\Delta_{min}$  ratio that is arbitrarily large than a  $|\vec{j}|$  that is arbitrarily large, and either will give rapid reconnection when the local magnetic Reynolds number reaches unity.

An obvious question about a singular current is what determines where it is located. The answer appears to be obvious for an ideal evolution of a magnetic field in a torus. In a topological torus, a mathematical singularity in the current density must form at a resonantly perturbed rational magnetic surface [16] to preserve the field-line topology as time  $t$  goes to infinity. On rational surfaces, magnetic field lines close after  $M$  toroidal and  $N$  poloidal circuits. Hahm and Kulsrud showed in Section III of [17] that in an ideal evolution the current density

increases only linearly in time near a rational surface. The width  $x$  of the shielding current becomes narrower as time increases, which makes the current density more singular with  $x/R \propto \tau_A/t$ , where  $\tau_A$  is the Alfvén transit time  $2\pi R/V_A$  of a torus with a major radius  $R$ . A current density that increases only linearly in time, which is the characteristic scaling in an ideal evolution, takes far too long to explain reconnection in the corona. The analogue of a rational surface in the corona is obscure. In a topological torus, the only place magnetic perturbations create current singularities is on rational surfaces.

Section II discusses stream functions for  $\vec{v}_t$  that produce bounded regions in which the streamlines are chaotic and the importance of the Frobenius norm as a measure of streamline separation. Section III derives the evolution of the magnetic field in the limit  $L/a \rightarrow \infty$ , a very tall cylinder compared to its radius, with  $|\vec{v}_t| \ll aV_A/L$ , where  $V_A$  is the Alfvén speed. Section IV considers the kink stability of the magnetic field. Section V determines the evolution of the magnetic flux enclosed by each magnetic field line, and Section VI the magnetic helicity contained within the cylinder. Section VII obtains the power that must be supplied by the photosphere to produce the flow represented by  $\vec{v}_t$ . Section VIII discusses the results.

## II. CHAOS IN THE DRIVING VELOCITY

The flow within the top end of the cylinder, which is given by Equation (3), obeys Hamilton's equations with the stream function  $h_t$  the Hamiltonian and  $(x, y)$  the canonical variables, where  $x = r \cos \theta$  and  $y = r \sin \theta$ .

The most important question about the Hamiltonian is whether its streamlines are chaotic. Neighboring chaotic streamlines have a separation  $\vec{\delta}$  that depends exponentially on time. This question can be answered streamline by streamline, as illustrated in Figure 2, using the Jacobian of Lagrangian coordinates  $\vec{x} = x(x_0, y_0, t)\hat{x} + y(x_0, y_0, t)\hat{y}$ , where  $(x_0, y_0)$  is the initial location of a streamline and  $(\partial \vec{x} / \partial t)_{x_0 y_0} \equiv d\vec{x} / dt = \vec{v}_t$ . To obtain an answer, two vector equations are integrated simultaneously;

$$\frac{d\vec{x}}{dt} = \vec{v}_t, \text{ where} \quad (4)$$

$$\vec{v}_t = -\frac{\partial h_t}{\partial y}\hat{x} + \frac{\partial h_t}{\partial x}\hat{y}, \text{ and} \quad (5)$$

$$\frac{d\vec{\delta}}{dt} = \vec{\delta} \cdot \vec{\nabla} \vec{v}_t. \quad (6)$$

Equation (4) is to be solved with the initial condition  $\vec{x}(0) = x_0\hat{x} + y_0\hat{y}$ , so solving that equation means

solving two coupled equations, one for  $dx/dt$  and one for  $dy/dt$ . Equation (6) is to be solved for two different initial conditions. The first solve is for  $\vec{\delta}_x = \delta_{xx}\hat{x} + \delta_{xy}\hat{y}$  with the initial condition  $\delta_{xx} = 1$  and  $\delta_{xy} = 0$ . The second solve is for  $\vec{\delta}_y = \delta_{yx}\hat{x} + \delta_{yy}\hat{y}$  with the initial condition  $\delta_{yx} = 0$  and  $\delta_{yy} = 1$ . Since Equation (6) for the evolution of the separation  $\vec{\delta}$  is linear, the initial separation can be taken to be unity without loss of generality. The Jacobian matrix for the starting point  $(x_0, y_0)$  is then

$$\frac{\partial \vec{x}}{\partial \vec{x}_0} \equiv \begin{pmatrix} \frac{\partial x}{\partial x_0} & \frac{\partial x}{\partial y_0} \\ \frac{\partial y}{\partial x_0} & \frac{\partial y}{\partial y_0} \end{pmatrix} = \begin{pmatrix} \delta_{xx} & \delta_{xy} \\ \delta_{yx} & \delta_{yy} \end{pmatrix}. \quad (7)$$

The determinant of the Jacobian matrix,  $\delta_{xx}\delta_{yy} - \delta_{yx}\delta_{xy}$  would be unity if there were no numerical errors. The Frobenius norm of the Jacobian matrix,  $\|\partial \vec{x} / \partial \vec{x}_0\|$ , gives the large singular value,  $\Lambda_u$ , of an SVD decomposition;

$$\begin{aligned} \left\| \frac{\partial \vec{x}}{\partial \vec{x}_0} \right\| &\equiv \sqrt{\delta_{xx}^2 + \delta_{xy}^2 + \delta_{yx}^2 + \delta_{yy}^2} \\ &= \sqrt{\Lambda_u^2 + 1/\Lambda_u^2}. \end{aligned} \quad (8)$$

The small singular value,  $\Lambda_s$ , is determined by the Jacobian, which is unity and equal to  $\Lambda_u \Lambda_s$ . When the flow is chaotic  $\Lambda_u$  becomes exponentially large and is essentially equal to the Frobenius norm,  $\|\partial \vec{x} / \partial \vec{x}_0\|$ , which is plotted in Figure 2b. A full SVD analysis gives additional information, the directions in both  $x_0, y_0$  space and in  $x, y$  space in which trajectories exponentiate apart and exponentiate together. The numerical accuracy of the calculations can be checked not only by the deviation of the Jacobian from unity, but also by simultaneously integrating one additional equation,  $dh_t/dt = \partial h_t / \partial t$ , and finding the deviation of  $h_t$  resulting from the integration from the actual  $h_t$ .

The Frobenius norm involves a sum of positive numbers and is less numerically demanding than the Jacobian, which is the difference between two numbers, each of order the Frobenius norm squared. The largest Frobenius norm in this paper is approximately  $10^8$ . The Jacobian can be the difference between two terms each of order  $10^{16}$ . The maximum error in the Jacobian is 15%. A more representative number is the standard deviation of the Jacobian from unity, which is 1.1%.

The probability distribution of the Frobenius norm is almost constant from the minimum, the smallest mathematically possible  $\sqrt{2}$ , to the largest  $8.5 \times 10^7$ , Figure 3c. The distribution function of exponentiations in the separation of magnetic field lines was calculated in 2014 for a related problem by Huang et al [18] with far fewer e-folds; their distribution was peaked.

The stream function can be chosen so that  $dr/dt$ ,  $d\theta/dt$ , and the radial gradient of  $d\theta/dt$  are all zero at  $r = a$ . This ensures that the streamlines can never strike the  $r = a$  boundary of the cylinder,  $\vec{v}_t = 0$  at  $r = a$ , and extremely large currents do not form in the plasma near  $r = a$ . A form for  $h_t$  that has this property is

$$h_t(r, \theta, t) = \tilde{h}(x, y, t) \left(1 - \frac{r^2}{a^2}\right)^3 e^{-\lambda^2 r^2/a^2}, \quad (9)$$

where  $\lambda^2$  is a constant. A large  $\lambda^2$  restricts the evolution-driven region to be far from the confining cylindrical walls. In the studies reported here,  $\lambda^2 = 0$ . The stream function is specified by giving  $\tilde{h}(x, y, t)$ . Keeping only the lowest order variations in  $x$  and  $y$ ,

$$\begin{aligned} \tilde{h} = \frac{a^2}{\tau} & \left[ c_0 \cos\left(\omega_0 \frac{t}{\tau}\right) + c_1 \frac{x}{a} \cos\left(\omega_1 \frac{t}{\tau}\right) \right. \\ & \left. + c_2 \frac{y}{a} \sin\left(\omega_2 \frac{t}{\tau}\right) \right\} + c_3 \frac{xy}{a^2} \cos\left(\omega_3 \frac{t}{\tau}\right) \right], \end{aligned} \quad (10)$$

where  $\omega_0$ ,  $\omega_2$ , and  $\omega_3$  are three frequencies, which are generally incommensurate, and  $c_0$ ,  $c_1$ ,  $c_2$ , and  $c_3$  are dimensionless amplitudes. For determining the chaotic region associated with a particular initial condition  $x_0, y_0$ , it is advantageous for the frequencies to be commensurate because then a Poincaré plot can be constructed using the time-periodic points. When the frequencies are commensurate,  $\tau$  is the periodicity time of  $\tilde{h}$ . The exponentiation, which is measured by the Frobenius norm, can be calculated whether the frequencies are commensurate or not.

A circular conducting-cylinder is easier to discuss and does not complicate the computations explored in this paper, but a cylinder with a square cross section simplifies more complete simulations. In a square cylinder, the factors of  $1 - r^2/a^2$  in Equation (9) are replaced by  $(1 - x^2/a^2)(1 - y^2/a^2)$ .

### III. EVOLUTION EQUATIONS

The evolution equations are simpler when the height of the cylinder is far greater than its radius,  $L/a \rightarrow \infty$ . The magnetic field then consists of a constant field  $B_0$  in the  $\hat{z}$  direction plus an orthogonal field produced by the velocity in the top surface.  $\vec{\nabla} \cdot \vec{B} = 0$  implies the magnetic field and the vector potential have the forms

$$\vec{B} = B_0 \left( \hat{z} + \hat{z} \times \vec{\nabla} H \right); \quad (11)$$

$$\vec{A} = B_0 \left( \frac{\hat{z} \times \vec{x}}{2} - H \hat{z} \right). \quad (12)$$

The constraint that the  $\hat{z}$ -directed field does not change is

$$\hat{z} \cdot \frac{\partial \vec{B}}{\partial t} = \hat{z} \cdot \vec{\nabla} \times (\vec{u} \times \vec{B}) \quad (13)$$

$$= -\vec{\nabla} \cdot (\hat{z} \times (\vec{u} \times \vec{B})) = 0, \text{ so} \quad (14)$$

$$\hat{z} \times (\vec{u} \times \vec{B}) = \hat{z} \times \vec{\nabla} (B_0 h) \quad (15)$$

to satisfy the divergence-free criterion of Equation (14). Implications are

$$\vec{u}_\perp = \hat{z} \times \vec{\nabla} h \text{ and} \quad (16)$$

$$\frac{\partial \vec{A}}{\partial t} = \vec{u}_\perp \times \vec{B} - B_0 \vec{\nabla} h. \quad (17)$$

The curl of the magnetic field of Equation (11) and the curl of the magnetic field line velocity  $\vec{u}_\perp$  of Equation (16) give the current and the vorticity along  $\vec{B}$ :

$$\nabla_\perp^2 H = K, \text{ where } K \equiv \frac{\mu_0 j_{||}}{B}, \text{ and} \quad (18)$$

$$\nabla_\perp^2 h = \Omega, \text{ where } \Omega \equiv \hat{z} \cdot \vec{\nabla} \times \vec{u}_\perp. \quad (19)$$

Equations (12) and (17) give two expressions for  $\vec{B} \cdot (\partial \vec{A} / \partial t)_\perp$ , which can be equated to obtain

$$\frac{\partial H}{\partial t} = \frac{\vec{B} \cdot \vec{\nabla} h}{B_0} \quad (20)$$

$$= \frac{\partial h}{\partial z} + (\hat{z} \times \vec{\nabla}_\perp H) \cdot \vec{\nabla}_\perp h \quad (21)$$

$$= \frac{\partial h}{\partial z} + \hat{z} \cdot (\vec{\nabla}_\perp h \times \vec{\nabla}_\perp H) \quad (22)$$

Appling  $\nabla_\perp^2$  to both sides of this equation,

$$\begin{aligned} \frac{\partial \nabla_\perp^2 H}{\partial t} = \frac{\partial \nabla_\perp^2 h}{\partial z} & + \hat{z} \cdot (\vec{\nabla}_\perp \nabla_\perp^2 h \times \vec{\nabla}_\perp H) \\ & + \hat{z} \cdot (\vec{\nabla}_\perp h \times \vec{\nabla}_\perp \nabla_\perp^2 H) \end{aligned} \quad (23)$$

$$= \frac{\vec{B}}{B_0} \cdot \vec{\nabla} (\nabla_\perp^2 h) - \vec{u}_\perp \cdot \vec{\nabla}_\perp (\nabla_\perp^2 H). \quad (24)$$

These equations and the definition of  $K$ , Equation (18), and of  $\Omega$ , Equation (19), imply

$$\left( \frac{\partial K}{\partial t} \right)_L = \left( \frac{\partial \Omega}{\partial \ell} \right)_L. \quad (25)$$

The subscript  $L$  on the partial derivatives implies the use of Lagrangian coordinates, which means  $x_0$  and  $y_0$  are held constant. The differential distance along a magnetic field line,  $d\ell$ , is equivalent to  $dz$  with  $x_0$  and  $y_0$  held constant. The implications of Equation (25) are extremely profound.

For simplicity, the plasma is assumed to have a negligible pressure and a constant density  $\rho$ , so force balance is  $\rho(\partial \vec{u}_\perp / \partial t + \vec{u}_\perp \cdot \vec{\nabla} \vec{u}_\perp) = \vec{f}_L$ , where  $\vec{f}_L = \vec{j} \times \vec{B}$  is the Lorentz force. The condition  $\vec{\nabla} \cdot \vec{j} = 0$  can be written as

$$\vec{B} \cdot \vec{\nabla} K = \vec{B} \cdot \vec{\nabla} \times \frac{\mu_0 \vec{f}_L}{B^2}, \text{ and} \quad (26)$$

$$\vec{\nabla} \times (\vec{u}_\perp \cdot \vec{\nabla} \vec{u}_\perp) = \vec{\nabla} \times (\vec{\Omega} \times \vec{u}_\perp) \quad (27)$$

$$= \vec{u}_\perp \cdot \vec{\nabla} \vec{\Omega} - \vec{\Omega} \cdot \vec{\nabla} \vec{u}_\perp, \quad (28)$$

where  $\vec{\Omega} = \Omega \hat{z}$ . The  $\hat{z}$  component of the curl of the force balance equation gives

$$\left( \frac{\partial \Omega}{\partial t} \right)_L = V_A^2 \left( \frac{\partial K}{\partial \ell} \right)_L, \text{ where } V_A^2 \equiv \frac{B_0^2}{\mu_0 \rho}. \quad (29)$$

Equations (25) and (29) together with the mixed partials theorem applied to either  $\Omega$  or  $K$  imply both  $\Omega$  and  $K$  obey the equation for shear Alfvén waves,  $(\partial^2 K / \partial t^2)_L = V_A^2 (\partial^2 K / \partial \ell^2)_L$ . Any variation in  $K$  along the magnetic field lines relaxes by Alfvén waves. Reconnection or ideal kink-instabilities will generally drive Alfvén waves. The inclusion of resistivity or viscosity causes these waves to diffuse across the magnetic field lines and produces wave decay [19]. In a completely ideal theory, the energy that goes into Alfvén waves will bounce back and forth forever, but they can be damped without directly affecting reconnection by adding viscosity or a drag-force to the force equation.

Equations (25) and (29) imply that during any period in which the evolution is slow compared to the Alfvén transit time  $L/V_A$  that

$$\left( \frac{\partial K}{\partial \ell} \right)_L = 0, \text{ and} \quad (30)$$

$$\left( \frac{\partial^2 \Omega}{\partial \ell^2} \right)_L = 0, \text{ so} \quad (31)$$

$$\Omega = \Omega_t(x_0, y_0, t) \frac{\ell}{L}, \text{ and} \quad (32)$$

$$\left( \frac{\partial K}{\partial t} \right)_L = \frac{\Omega_t(x_0, y_0, t)}{L}, \text{ where} \quad (33)$$

$$\Omega_t \equiv \hat{z} \cdot \vec{\nabla} \times \vec{v}_t. \quad (34)$$

The flow of the top perfectly-conducting surface is specified, and  $\Omega_t(x_0, y_0, t)$  is obtained from that specified flow alone. For an example of a calculation of the evolution of  $KL$ , see Figure 2c.

Equations (18) and (33) provide a Poisson equation,  $\nabla_\perp^2 H = K$ , for  $H$  and an expression for  $K$ , which can be solved for each value of  $z$  and  $t$ . The boundary condition is that the component of  $\vec{\nabla}_\perp H$  that is tangential to the wall must vanish, otherwise

the magnetic field would penetrate the perfectly conducting wall.

For any physically reasonable flow,  $\Omega_t(x_0, y_0, t)$  is bounded,  $|\Omega_t| \leq \Omega_{max}$ , which can be easily calculated analytically for any analytic  $h_t(x, y, t)$ . An extremely important result is that the maximum current density along the magnetic field  $j_{||}$  satisfies

$$K_{max} \leq \frac{\Omega_{max}}{L} t. \quad (35)$$

The probability distribution function for  $K$ , Figure 3d, is exponential with a peak at zero, which is very different in form for that of the Frobenius norm, which is almost constant from the smallest possible value,  $\sqrt{2}$ , to the largest on any of the ten thousand trajectories,  $8.5 \times 10^7$ , Figure 3c.

When the specified flow in the top surface is chaotic, the spatial derivatives of  $K$  will tend to become exponentially large in some directions and exponentially small in others, but the current density itself is strictly bounded by a linear increase in time. In other words, the current density within the plasma lies in ribbons with a decreasing thickness in one direction across  $\vec{B}$ , an increasing width in the other direction across  $\vec{B}$ , and a constant amplitude along  $\vec{B}$ . This thinning while increasing in width is illustrated by the top row of Figure 4.

The anisotropy of the spatial derivatives of  $K$  follows from the exponentially large anisotropy of the spatial derivatives of  $\Omega_t(x_0, y_0, t)$  in  $x_0, y_0$  space. For simple stream functions  $h_t(x, y, t)$ , such as those defined by Equation (10),  $\Omega_t(x, y, t) = \nabla^2 h_t$  has a simple and smooth variation in  $x, y$  coordinates. But, the streamlines,  $x(x_0, y_0, t)$  and  $y(x_0, y_0, t)$ , of a two-dimensional, divergence-free chaotic flow separate exponentially in time in one direction, which implies they must exponentially converge in the other. For a divergence-free flow, the two singular values of the Jacobian matrix  $\partial \vec{x} / \partial \vec{x}_0$  must be inverses of each other. The spatial derivatives of  $\Omega_t(x_0, y_0, t)$  in the converging direction become exponentially large and those in the diverging direction become exponentially small.

Employing Equation (33),  $\Omega_t(x_0, y_0, t)$  determines  $K(x_0, y_0, z, t)$ . Consequently, the streamlines of  $\vec{v}_t$  determine the properties of  $K(x_0, y_0, z, t)$  throughout the plasma. Figure 2c illustrates how a hundred magnetic field lines that initially had nearby  $x_0, y_0$  locations develop a large variation in  $KL$ . As can be seen in Figure 4, there is only a weak correlation between regions where  $|K|$  is large and where the Frobenius norm is large. This is consistent with the results of Reid et al [13] that the quasi-squashing factor, which is determined by the Frobenius norm, Equation (8), has a little correlation with a large  $\int \eta j_{||} d\ell = B_0(\eta/\mu_0)KL$ .

Magnetic field lines that have distant intersection points with the bottom surface of the cylinder,  $x_0, y_0$  and  $x'_0, y'_0$  can interchange their intersections on the top surface if anywhere along their trajectories they are sufficiently close to be indistinguishable. This means they come closer than  $c/\omega_{pe}$  or the distance through which they resistively diffuse,  $\sqrt{(\eta/\mu_0)t}$

The current density required for a large exponentiation is relatively small [20]. The minimum number of exponentiations is given by the properties of  $h_t$ , but more are possible. The separation  $\vec{\Delta} = \Delta_x \hat{x} + \Delta_y \hat{y}$  between two neighboring magnetic field lines obeys  $d\vec{\Delta}/dz = \vec{\Delta} \cdot \vec{\nabla} \hat{b}$ , where  $\hat{b} = \hat{z} + \hat{z} \times \vec{\nabla} H$ . That is,

$$\frac{d\Delta_x}{dz} = -\frac{\partial^2 H}{\partial x \partial y} \Delta_x - \frac{\partial^2 H}{\partial y^2} \Delta_y \quad (36)$$

$$\frac{d\Delta_y}{dz} = \frac{\partial^2 H}{\partial x^2} \Delta_x + \frac{\partial^2 H}{\partial x \partial y} \Delta_y. \quad (37)$$

An exact answer for the separation requires a solution of the equation  $\nabla_{\perp}^2 H = K$ . But, the typical magnitude of the second derivatives of  $H$ , which appear in Equations (36) and (37) is  $K$ , which suggests that the number of e-folds is typically of order  $KL$ . Figure 2 illustrates this scaling as does Figure 3a. The scaling holds for the ensemble averages but does not hold field line by field line, which is another way of saying that the correlation between the magnitude of the Frobenius norm and the current is weak. A current along a magnetic field line affects not only the Hamiltonian and its derivatives on that line but elsewhere as well.

#### IV. KINK STABILITY

The current flowing along the magnetic field lines causes the lines to twist through an angle  $\Theta = KL/2$  from one end of the cylinder to the other. When the twist has a smooth variation with radius, Hood and Priest [21] found the magnetic field becomes kink unstable when  $\Theta$  is greater than a critical value, which in their calculations lay in the range  $2\pi$  to  $6\pi$ . Studies of the onset of reconnection in the model of Figure 1 are much simpler when ideal kink instabilities are not an issue.

The largest  $KL$  values in Figure 2c correspond to  $\Theta \approx 25\pi$ , but the current  $K$  has an extremely complicated spatial distribution, not only in magnitude but also in sign; spatial averages are far smaller than the maximum value. As will be discussed, the anisotropy of the derivatives of  $K$  across the magnetic field lines and the smallness of the spatial averages of  $K$  makes the system highly stable to kinks.

It is not required that  $K$ , or equivalently the twist  $\Theta$ , have a small spatial averages when the flow is chaotic. The spatially averaged twist  $\Theta$  can be made arbitrarily large by choosing  $c_0$  to be large and  $\omega_0$  to be either zero or small in Equation (10) for  $\tilde{h}$ . The choice  $c_0 = 0$  was made to show that a smooth twisting motion need not be large to obtain chaos.

Even when  $c_0 = 0$ , the spatial average of  $K$  over small regions can be non-zero. This is illustrated by Figure 2c and by the first row of Figure 4.

When the stream function is chosen so the flow is chaotic but with a large spatially-averaged  $K$ , the resulting magnetic field will generally evolve not only into a kinked but also into an eruptive state. As shown in Section VI, the evolution properties of magnetic helicity imply the spatial and temporal average of  $h_t$  must be zero for a non-eruptive steady-state solution for the magnetic field when  $R_m \gg 1$ —no matter how spatially concentrated the current may become. Consequently, non-eruptive chaotic models tend to have spatially complicated distributions of  $\Theta$  in which  $\Theta$  has both signs and a near-zero spatial average as in the  $\vec{v}_t$  example used in Figure 2.

As discussed in Section V.B.1 of [22], the stability of force-free equilibria can be determined using the perturbed equilibrium equation  $\vec{\nabla} \times \delta \vec{B} = (\mu_0 \delta j_{||}/B) \vec{B}$ , where  $\delta \vec{B} = \vec{\nabla} \times (\delta A_{||} \hat{z})$ . The perturbed parallel current is determined by the constancy of  $K \equiv \mu_0 j_{||}/B$  along magnetic field lines, which in linear order in the perturbation implies  $\vec{B} \cdot \vec{\nabla} \delta K + \delta \vec{B} \cdot \vec{\nabla} K = 0$ . Stability is determined by whether it takes positive or negative energy to drive a perturbation that obeys the equations

$$\nabla_{\perp}^2 \delta A_{||} = -\delta K B_0; \quad (38)$$

$$B_0 \left( \frac{\partial \delta K}{\partial \ell} \right)_{x_0 y_0} = \hat{z} \cdot (\vec{\nabla}_{\perp} A_{||} \times \vec{\nabla}_{\perp} K). \quad (39)$$

The system is at marginal stability when  $\delta K$  is just strong enough to produce a solution  $\delta A_{||}$  that fits within the perfectly conducting cylindrical walls. The implication is that when Equation (38) is multiplied by  $\delta A_{||}$ , then at marginal stability

$$\int \left\{ (\vec{\nabla}_{\perp} \delta A_{||})^2 - \delta K \delta A_{||} B_0 \right\} d^3 x = 0. \quad (40)$$

When  $\delta K$  has only a rapid spatial variation, as it does when  $K$  does, then  $\delta A_{||}$  must also have a rapid variation to avoid a self-cancelation of the destabilizing term  $\delta K \delta A_{||}$  in Equation (40). Equation (39) for  $\delta K$  involves two spatial derivatives across  $\vec{B}$  and one might think they could be large and balance the stabilizing effect of the two spatial derivatives in

$(\vec{\nabla}_\perp \delta A_{||})^2$ , but that is not the case. The two spatial derivatives across  $\vec{B}$  in the equation for  $\delta K$  are orthogonal and the spatial derivatives of  $K$  in the two directions across the magnetic field lines tend to be of exponentially different magnitudes, so the large term in  $\vec{\nabla}_\perp K$  forces a large spatial derivative in  $\delta A_{||}$ , which quadratically enhances  $(\vec{\nabla}_\perp \delta A_{||})^2$  but only linearly enhances  $\delta K$ .

## V. MAGNETIC FLUX

The change in the magnetic flux associated with a particular magnetic field line  $\psi(x_0, y_0, t)$  is the integral from one perfectly conducting surface to the other,  $\partial\psi/\partial t = -\int \vec{E} \cdot d\vec{\ell}$ . When the cylindrical conductor is stationary and the plasma is resistive, the flux decays as  $\partial\psi/\partial t = -\int \eta \vec{j} \cdot d\vec{\ell}$ .

As was shown in the derivation of Equation (17) for  $\partial\vec{A}/\partial t$ , the effective inductive electric field along the magnetic field is  $-\vec{B} \cdot (\partial A/\partial t) = \vec{B} \cdot (B_0 \vec{\nabla} h)$ , which gives a change in the flux,  $\partial\psi/\partial t = -\int \vec{E} \cdot d\vec{\ell}$ , or

$$\frac{\partial\psi}{\partial t} = -B_0 h_t((x_0, y_0, t)) \quad (41)$$

since the at the top of the cylinder  $h = h_t$ .

The appearance of  $B_0 h_t$  in the electric-field integral can be understood using the expression  $\vec{E} = -\vec{v}_t \times \vec{B}_0$  for the electric field in the flowing conductor when observed from a stationary frame of reference. The velocity is  $\vec{v}_t = \hat{z} \times \vec{\nabla} h_t$  and  $\vec{B}_0 = B_0 \hat{z}$ , so  $\vec{E} = -B_0 \vec{\nabla}_\perp h_t$ . The electromotive force from the intersection point of the field line to a stationary point, where  $h_t = 0$ , is  $B_0 h_t$ .

The rate at which plasma resistivity destroys magnetic flux is  $\mathcal{E}_\eta = \int \eta j_{||} d\ell$ . Since  $K = \mu_0 j_{||}/B$  is constant along a magnetic field line,  $\mathcal{E}_\eta = B_0(\eta/\mu_0)K(x_0, y_0, t)L$ . Equation (33) implies  $\partial\mathcal{E}_\eta/\partial t = -B_0(\eta/\mu_0)\Omega_t(x_0, y_0, t)$ . Since  $\Omega_t = \nabla^2 h_t$ , the ratio of flux creation to flux destruction is

$$\left| \frac{2\partial h_t/\partial t}{(\eta/\mu_0)\nabla^2 h_t} \right| \approx R_m \sim 10^{12} \quad (42)$$

in the solar corona.

## VI. MAGNETIC HELICITY

As will be shown, an argument based on magnetic helicity implies a long-term relevant solution to the problem outlined in Figure 1 requires the long-term spatial and temporal average of  $h_t$  to be zero. When

the average of  $h_t$  is zero over a chaotic region, the interchange of penetration points implies the poloidal magnetic flux associated with a field line  $x_0, y_0$  fluctuates but has no systematic increase.

Chaotic streamlines can cause two field lines that penetrate the bottom of the cylinder at two distant points  $x_0, y_0$  and  $x'_0, y'_0$  to interchange their penetration points through the top plane due to exponentially small non-ideal effects.

Equation (52) for the evolution of the magnetic helicity limits the degree to which a magnetic field driven as in Figure 1 can be simplified by magnetic field lines exchanging connections even if the current density were to obtain arbitrarily high local values by being concentrated in thin sheets. As has been shown, the maximum current density does not tend to have the enhancement by a factor of order  $1/R_m$  that would be required for the loop voltage to balance the poloidal flux creation. But, even if it did the rate of helicity dissipation would not be significantly enhanced, Equation (52). Magnetic turbulence can reduce the magnetic energy, but not the helicity [23, 24] as  $R_m \rightarrow \infty$ .

Equation (50) for the rate of helicity increase implies that unless the stream function integrated over each chaotic region,  $\int h_t d\ell$ , has a zero time average, the magnetic helicity can increase without limit. In the model of this paper, the perfectly conducting cylindrical boundary conditions will keep the system confined no matter how strong or contorted the magnetic field may become. But, in a natural system, such as the solar corona, a drive  $h_t$  that does not have a zero long-term average will presumably cause the eruption of a magnetic flux tube.

The derivation of the helicity evolution equation starts with the definition of the magnetic helicity enclosed by the cylinder,

$$\mathcal{K} \equiv \int \vec{B} \cdot \vec{A} d^3x. \quad (43)$$

Equations (11) and (12) together with  $\vec{\nabla} \cdot \vec{x}_\perp = 2$  imply  $\vec{B} \cdot \vec{A} = B_0^2(-2H + \vec{\nabla}_\perp \cdot (H\vec{x}_\perp))$ . The helicity is then

$$\mathcal{K} = -2B_0^2 \int H d^3x. \quad (44)$$

The time derivative of the helicity is calculated using

$$\begin{aligned} \frac{\partial \vec{B} \cdot \vec{A}}{\partial t} &= \vec{B} \cdot \frac{\partial \vec{A}}{\partial t} + \vec{A} \cdot \vec{\nabla} \times \frac{\partial \vec{A}}{\partial t} \\ &= 2\vec{B} \cdot \frac{\partial \vec{A}}{\partial t} - \vec{\nabla} \cdot \left( \vec{A} \times \frac{\partial \vec{A}}{\partial t} \right) \text{ and (45)} \end{aligned}$$

$$\vec{A} \times \frac{\partial \vec{A}}{\partial t} = -B_0^2 \frac{\vec{x}_\perp}{2} \frac{\partial H}{\partial t}, \text{ so} \quad (46)$$

$$\frac{\partial \vec{B} \cdot \vec{A}}{\partial t} = 2\vec{B} \cdot \frac{\partial \vec{A}}{\partial t} + \vec{\nabla} \cdot \left( B_0^2 \frac{\vec{x}_\perp}{2} \frac{\partial H}{\partial t} \right) \} \quad (47)$$

The side of the cylinder is a rigid perfect conductor, so  $\partial H/\partial t = 0$  within its sides. Consequently,

$$\frac{d\mathcal{K}}{dt} = 2 \int \vec{B} \cdot \frac{\partial \vec{A}}{\partial t} d^3x \quad (48)$$

$$= -2B_0 \int \vec{\nabla} \cdot (h\vec{B}) d^3x \quad (49)$$

$$= -2B_0^2 \int h_t da_t, \quad (50)$$

using Equation (17) with  $da_t = r dr d\theta$  the area integral over the top of the cylinder. Since the magnetic field lines are tied to the flow of the perfectly conducting top,  $h = h_t$  within the top surface.

The effect of resistivity on the helicity is obtained by letting  $\partial \vec{A}/\partial t = \vec{u}_\perp \times \vec{B} - \vec{\nabla} h - \eta \vec{j}$ , then Equation (50) implies

$$\frac{d\mathcal{K}}{dt} = -B_0^2 \int \left( h_t + \frac{\int \eta j_{||} d\ell}{B_0} \right) da_t \quad (51)$$

$$= -B_0^2 \int \left( h_t + \int \frac{\eta}{\mu_0} K d\ell \right) da_t \quad (52)$$

The effect of resistivity on the helicity evolution is given by the volume-averaged  $K$ , and is therefore unaffected by  $K$  being concentrated. When the evolution is slow compared to the Alfvén transit time  $K$  is independent of  $\ell$ , and the ratio of helicity input to its resistive destruction is

$$\left| \frac{h_t}{\int \frac{\eta}{\mu_0} K d\ell} \right| \sim \frac{av_t}{\frac{\eta}{\mu_0} L \frac{v_t t}{a^2 L}} \sim \left( \frac{\mu_0 a^2}{\eta} \right) \left( \frac{v_t}{a} \right) \frac{a/v_t}{t} \quad (53)$$

$$\sim R_m \frac{a/v_t}{t}, \quad (54)$$

while  $R_m \sim 10^{12}$  in the corona. To extreme accuracy, resistivity has no effect on the rate of helicity increase in the corona.

## VII. POWER INPUT

The condition  $\vec{\nabla} \cdot \vec{j} = 0$  implies that the Lorentz force  $\vec{f}_L = \vec{j} \times \vec{B}$  obeys Equation (26). Using

$$\vec{B} \cdot \vec{\nabla} K = B_0 \frac{\partial K}{\partial \ell} = -K\delta(\ell - L) \quad (55)$$

$$= B_0 \frac{\mu_0}{B_0^2} \hat{z} \cdot \vec{\nabla} \times \vec{f}_L, \quad (56)$$

$$\hat{z} \cdot \vec{\nabla} \times \vec{f}_L = -\frac{B_0^2}{\mu_0} K\delta(\ell - L). \quad (57)$$

The power required to maintain the flow in the top of the cylinder is

$$\begin{aligned} \mathcal{P} &= - \int \vec{v}_t \cdot \vec{f}_L d^3x \quad (58) \\ &= - \int \hat{z} \cdot (\vec{\nabla} h_t \times \vec{f}_L) d^3x \\ &= - \int \hat{z} \cdot \left( \vec{\nabla} \times (h_t \vec{f}_L) - h_t \vec{\nabla} \times \vec{f}_L \right) d^3x \\ &= - \int \hat{z} \cdot \left( -\vec{\nabla} (h_t \hat{z} \times \vec{f}_L) \right. \\ &\quad \left. + \frac{B_0^2}{\mu_0} h_t K \delta(\ell - L) \right) d^3x \\ &= -\frac{B_0^2}{\mu_0} \int h_t(x_0, y_0, t) K(x_0, y_0, t) dx_0 dy_0. \quad (59) \end{aligned}$$

The integrand becomes extremely spatially complicated at time evolves but not very large.

## VIII. DISCUSSION

The prevalence of magnetic reconnection in situations in which effects that cause a departure from an ideal evolution are arbitrarily small suggests the cause of reconnection must be within the ideal evolution equation itself. Indeed it is [8].

In an ideal evolution, the magnetic field lines move with the velocity  $\vec{u}_\perp$  of Equation (1). As Schindler, Hesse, and Birn [3] stated in 1988, resistivity  $\eta$  can only compete with the ideal evolution in a region  $\Delta_d$  that is sufficiently narrow across the magnetic field lines that the local magnetic Reynolds number,  $R_\ell = (\mu_0 u_\perp / \eta) \Delta_d \sim 1$ . The actual scale  $a$  across the magnetic field lines in many problems of practical interest gives a Reynolds number  $R_m = (\mu_0 u_\perp / \eta) a$  that is many orders of magnitude larger than unity—in both natural and laboratory plasmas. In the solar corona  $R_m \sim 10^{12}$ . There are two ways to produce the  $a/\Delta_d \sim R_m$  required by the argument of Schindler et al.

The first possibility, which is the dominant reconnection paradigm and the only one considered by Schindler et al, is that the ideal magnetic evolution creates and maintains layers of intense current density  $j \sim B_{rec}/\mu_0 \Delta_d$ , where  $B_{rec}$  is the reconnecting magnetic field. One problem with this possibility is that in an ideal evolution the current density tends to increase only linearly in time. A linear increase in the current density by a factor  $R_m$  takes far too long to explain many natural phenomena. As discussed in the Introduction, the growth in current density is linear even in ideal flows that are known to create a singular current density as time goes to infinity—flows that have a resonant interaction with a rational magnetic surface in a torus.

The second possibility, which has aroused little interest, notes that an ideal flow  $\vec{u}_\perp$  naturally increases the ratio of the maximum to the minimum separation,  $\Delta_{\max}/\Delta_{\min}$ , between two arbitrarily chosen magnetic lines. This increase is characteristically exponential when the field-line trajectories are calculated at different points in time. Reconnection occurs when  $\Delta_{\max}/\Delta_{\min} \sim R_m$  with  $\Delta_{\min} = \Delta_d$ , the spatial scale over which field line distinguishability is lost, and  $\Delta_{\max} \sim a$ , the system scale.

Unlike a localized current density,  $\Delta_{\max}/\Delta_{\min}$  becomes large over extended regions. Nonetheless, the exponential increase differs from one pair of magnetic field lines to another—even over small regions, Figure 2b. Magnetic field lines that have the largest exponentiations reconnect first, which can break force balance and cause Alfvénic relaxations. The associated ideal field-line velocity  $\vec{u}_\perp$  causes an increase in  $\Delta_{\max}/\Delta_{\min}$  on an Alfvénic time scale for pairs of magnetic field lines in other regions.

All that is required to produce reconnection by the Parker and Krook definition [2], the “*severing and reconnection of lines of force*,” is that magnetic field lines become indistinguishable on some spatial scale  $\Delta_d$  and that the exponentiation of field-line separation magnify the indistinguishability scale to the scale over which reconnection occurs.

A simple way to drive an ideal magnetic evolution is by a flow  $\vec{v}_t$  in a perfectly conducting surface, as in the model of Figure 1. To minimize the energy required to drive the flow, it must be divergence free with the streamlines defined by a stream function,  $\vec{v}_t = \hat{z} \times \vec{\nabla} h_t$ . The stream function is a Hamiltonian  $h_t(x, y, t)$  for the streamlines,  $dx/dt = -\partial h_t/\partial y$  and  $dy/dt = \partial h_t/\partial y$ . Although the streamlines defined by  $h_t$  are deterministic, Section II demonstrates that simple and slowly varying stream functions  $h_t(x, y, t)$  have separations between neighboring streamlines that increase exponentially with time. In mathematics this is called deterministic chaos. The primary requirement for the exponentiation is that  $h_t(x, y, t)$  have a non-trivial dependence on all three of its variables. As explained in Section II, the level of streamline exponentiation that is reached after a time  $t$  in the immediate vicinity of an arbitrarily chosen streamline, the Frobenius norm of a Jacobian matrix, can be calculated using a set of coupled ordinary differential equations.

Magnetic field lines are defined at a given time  $t$ . When the magnetic lines that cross an ideal plasma intercept two perfectly conducting surfaces—one fixed and one moving, the neighboring lines must exponentiate apart as much as the streamlines in the flowing surface have by the time  $t$ . Since streamline exponentiation increases forever with time, Figure 3a, the exponentiation of the magnetic field lines

will cause reconnection on a time scale that is only logarithmically dependent on smallness of the spatial scale  $\Delta_d$  on which magnetic field lines become indistinguishable.

When the evolution time, which is defined by the spatial gradient of the flow  $\vec{v}_t$ , is long compared to the time for an Alfvén wave to propagate from one magnetic field line interception to the other, the stream function determines the most important properties of the ideal evolution: the exponentially increasing separation between neighboring lines, the force-free current profile throughout the plasma, the power required to drive the flow, and the ratio of the resistive destruction in the magnetic flux relative to its creation, which is approximately  $1/R_m$ . Section VI demonstrated that unless  $h_t(x, y, t)$  has a zero spatial and temporal average in a region, the magnetic helicity increases without limit in the volume occupied by the magnetic field lines that strike that region. When  $R_m \gg 1$ , magnetic helicity cannot be destroyed faster than it is created in such regions—even by turbulence—and the result must be the ejection of a magnetic flux tube, called a plasmoid, from the region.

Many may be surprised by the spatial complexity of the current density produced by even a simple driving velocity  $\vec{v}_t$  in a force-free plasma, Figure 2c. Observations of spatial complexity in the current density are not a proof of turbulence. Nearby magnetic field lines can have currents flowing in opposite directions.  $K = \mu_0 j_{||}/B$  increases only linearly in time and forms ribbons along the magnetic field that tend to widen exponentially and thin as one over the exponential, Figure 4. As discussed in Appendix E of [9], the currents produced by the more localized photospheric motions could produce runaway electrons and explain the hot corona.

To be consistent with Ampere’s law, the current density must have a value approximately proportional to the logarithm of the exponentiation factor [20]. The exponentiation factor is the Frobenius norm of a Jacobian matrix. This property is illustrated in Figure 3a and requires the current density be enhanced by factor of  $\ln(R_m)$  above its characteristic value before reconnection due to exponentially enhanced resistive diffusion can compete with evolution. An enhancement of the current density by  $\ln(R_m) \sim \ln(10^{12}) \approx 28$  is far more credible than an enhancement by  $R_m \sim 10^{12}$ . In an ideal evolution, the increase in the current density is approximately proportional to time divided by the ideal-evolution time scale as illustrated in Figures 2c and 3a.

In the application of the model of Figure 1 to the solar corona, the velocity  $\vec{v}_t$  represents the motion imposed on coronal loops by the photosphere. Although the example of  $\vec{v}_t$  discussed here had a

very simple and smooth spatial and temporal dependence, realistic footpoint motions of coronal loops are far more complicated, which makes them more prone to chaos. However, the parts of the footpoint motion that cause the most rapid development of states in which large-scale reconnection is inevitable have a spatial scale comparable to the region  $a$  over which reconnection will take place.

The calculations made in this paper demonstrate that a magnetic field reaches a state in which reconnection is inevitable on a time scale that is comparable to the ideal evolution time scale, even when drive for the evolution is simple. Nonetheless, more complete simulations, such as those of Reid et al [7], are required for a more complete understanding of how the reconnection proceeds. Such simulations are numerically simpler when the circular cylinder of Figure 1 is replaced by a cylinder of square cross section that encloses the volume with  $|x| < a$ ,  $|y| < a$ , and  $0 < z < L$ . As mentioned at the end of Sec-

tion II, the only significant modification required is a change in the factors of  $1 - r^2/a^2$  in Equation (9) to  $(1 - x^2/a^2)(1 - y^2/a^2)$ .

## Acknowledgements

This work was supported by the U.S. Department of Energy, Office of Science, Office of Fusion Energy Sciences under Award Numbers DE-FG02-95ER54333, DE-FG02-03ER54696, DE-SC0018424, and DE-SC0019479.

## Data availability statement

The data that support the findings of this study are available from the corresponding author upon reasonable request.

---

[1] W. A. Newcomb, *Motion of magnetic lines of force*, Ann. Phys. **3**, 347 (1958).

[2] E. N. Parker and M. Krook, *Diffusion and severing of magnetic lines of force*, Ap. J. **124**, 214 (1956).

[3] K. Schindler, M. Hesse, and J. Birn, *General magnetic reconnection, parallel electric-fields, and helicity*, Journal of Geophysical Research—Space Physics **93**, 5547 (1988).

[4] E. N. Parker EN (1972) *Topological dissipation and the small-scale fields in turbulent gases*, Astrophys. J. **174**, 499 (1972).

[5] David I. Pontin and Gunnar Hornig, *The Parker problem: existence of smooth force-free fields and coronal heating*, Living Reviews in Solar Physics **17**, 5 (2020).

[6] A. H. Boozer, *Why fast magnetic reconnection is so prevalent*, Journal of Plasma Physics **84**, 715840102 (2018).

[7] J. Reid, A. W. Hood, C. E. Parnell, P. K. Browning, and P. J. Cargill, *Coronal energy release by MHD avalanches: continuous driving*, Astronomy and Astrophysics **615**, A84 (2018).

[8] A. H. Boozer, *Fast magnetic reconnection and the ideal evolution of a magnetic field*, Phys. Plasmas **26**, 042104 (2019).

[9] A. H. Boozer, *Fast magnetic reconnection and particle acceleration*, Phys. Plasmas **26**, 082112 (2019).

[10] A. H. Boozer, *Magnetic Reconnection with null and X-points*, Phys. Plasmas **26**, 122902 (2019).

[11] A. H. Boozer, *Magnetic reconnection and thermal equilibration*, posted on ArXiv <https://arxiv.org/pdf/2009.14048.pdf>.

[12] E. Pariat, S. K. Antiochos, and C. R. DeVore, *A model for solar polar jets*, Ap. J. **691**, 61 (2009).

[13] J. Reid, C. E. Parnell, A. W. Hood, and P. K. Browning, *Determining whether the squashing factor,  $Q$ , would be a good indicator of reconnection in a resistive MHD experiment devoid of null points*, Astronomy and Astrophysics **633**, A92 (2020).

[14] E. R. Priest and P. Démoulin, *Three-dimensional magnetic reconnection without null points: 1. Basic theory of magnetic flipping*, J. Geophys. Res., **100**, 23443 (1995).

[15] V. S. Titov, G. Hornig, and P. Démoulin, *Theory of magnetic connectivity in the solar corona*, J. Geophys. Res., **107**, 1164 (2002).

[16] A. H. Boozer and N. Pomphrey, *Current density and plasma displacement near perturbed rational surfaces*, Phys. Plasmas **17**, 110707 ??(2010).

[17] T. S. Hahm and R. M. Kulsrud, *Forced magnetic reconnection*, Phys. Fluids **28**, 2412 (1985).

[18] Yi-Min Huang, A. Bhattacharjee, and A. H. Boozer, *Rapid change of field line connectivity and reconnection in stochastic magnetic fields*, Ap. J. **793**, 106 (2014).

[19] A. H. Boozer, *Flattening of the tokamak current profile by a fast magnetic reconnection with implications for the solar corona*, Phys. Plasmas **27**, 102305 (2020).

[20] A. H. Boozer, *Separation of magnetic field lines*, Phys. Plasmas **19**, 112901 (2012).

[21] A. W. Hood and E. R. Priest, *Kink instability of solar coronal loops as the cause of solar flares*, Solar Physics **64**, 303 (1979).

[22] A. H. Boozer, *Physics of magnetically confined plasmas*, Rev. Mod. Phys. **76**, 1071 (2004).

[23] J. B. Taylor, *Relaxation of Toroidal Plasma and Generation of Reverse Magnetic Fields*, Phys. Rev. Lett. **33**, 1139 (1974).

[24] M. A. Berger, *Rigorous new limits on magnetic helicity dissipation in the solar corona*, Geophysical and Astrophysical Fluid Dynamics, **30**, 79 (1984).